Construction and Building Materials 502 (2025) 144246

Contents lists available at ScienceDirect

Construction and Building Materials

journal homepage: www.elsevier.com/locate/conbuildmat

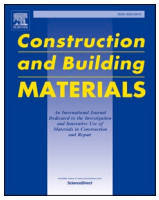

Piezoresistivity and mechanical performance of self-sensing cement-based sensors under the influence of seawater

Zhizhong Deng [a,*], Aziz Hasan Mahmood [a], Quang Dieu Nguyen [a,*], Wengui Li [a,b], Daichao Sheng [a]

[a] School of Civil and Environmental Engineering, University of Technology Sydney (UTS), Sydney, NSW 2007, Australia
[b] Centre for Infrastructure Engineering and Safety, School of Civil and Environmental Engineering, The University of New South Wales (UNSW), NSW 2052, Australia

ARTICLE INFO

Keywords:
Seawater self-sensing cementitious sensors
Ion concentration
Percolation thresholds
Ion conduction

ABSTRACT

This study investigates the integration of multi-walled carbon nanotubes (MWCNTs) as conductive fillers and self-sensing sensors in cementitious composites. Seawater (SW) was used as mixing water to evaluate its influence on the self-sensing performance, percolation thresholds, and mechanical properties of the composites. A range of analytical techniques: Thermogravimetric Analysis (TGA), X-ray Diffraction (XRD), Inductively Coupled Plasma (ICP), Scanning Electron Microscopy (SEM), and Energy-Dispersive X-ray Spectroscopy (EDS) were employed to examine hydration products and microstructural characteristics. SW enhances early-age hydration and compressive strength, as evidenced by increased heat evolution. The percolation threshold was found to vary with MWCNT dosage and ion concentration in the pore solution. Notably, composites containing 0.7 wt% MWCNTs and 50 wt% SW exhibited the highest fractional change in electrical resistance, indicating superior self-sensing capability. These findings offer valuable insights into the development of seawater-based, self-sensing cementitious materials for smart infrastructure and structural health monitoring applications.

1. Introduction

Cement-based self-sensing sensors have attracted increasing attention due to their capability to enable real-time structural health monitoring (SHM) and weigh-in-motion traffic detection in civil infrastructure [1–3]. Piezoresistivity is an indicative property of self-sensing cementitious sensors; more conductive composites result in a lower piezoresistivity. The conductive filler is one of the key components governing the piezoresistive behaviour of self-sensing cementitious composites. Various conductive fillers have been investigated, including graphite platelets, carbon black (CB), carbon fibres (CF), carbon nanotubes (CNTs), and multi-walled carbon nanotubes (MWCNTs) [4–6]. Due to the high surface area and aspect ratio, the MWCNTs showed an excellent electrical performance in self-sensing cement composites [7]. Incorporating conductive fillers enables cementitious sensors to exhibit high sensitivity to applied load variations. Moreover, these self-sensing composites demonstrate excellent compatibility and durability when integrated with conventional concrete structures [8]. As cement-based self-sensing sensors can be applied in weigh-in-motion systems, it has high application potential for traffic condition detection, especially in the critical parts of pavements.

With the rapid pace of urbanisation, the global demand for cementitious materials continues to increase, as cement remains a fundamental component of modern infrastructure. As the second most consumed material worldwide, cementitious composites are produced and utilised on a massive scale, with an estimated annual consumption of approximately 30 billion tons [9–11]. The manufacturing of these composites is highly reliant on the use of water. A cubic meter of concrete consumes about 150 L of water [12]. This amounts to about 16.6 billion cubic meters of water being used for concrete production per year [13,14]. This level of production accounts for approximately 9 % of global industrial water withdrawal. Such substantial water consumption is particularly concerning in regions already experiencing water stress. Projections indicate that by 2050, nearly 75 % of the freshwater required for cementitious composite production will be demanded in areas affected by water scarcity [13,15]. It has become vital to investigate alternative water sources to avoid such water stress.

Ocean resources appear abundant in both minerals and energy reserves compared with the limited availability of terrestrial resources. The utilisation of marine resources has been trialled in recent

* Corresponding authors.
E-mail addresses: zhizhong.deng@student.uts.edu.au (Z. Deng), quangdieu.nguyen@uts.edu.au (Q.D. Nguyen).

https://doi.org/10.1016/j.conbuildmat.2025.144246
Received 27 July 2025; Received in revised form 12 October 2025; Accepted 25 October 2025
Available online 11 November 2025

engineering projects [16]. The seawater (SW) covers 71 % of the Earth's surface, accounting for about 1.386 billion cubic kilometres of resources. SW contains a high concentration of dissolved ions that can accelerate reinforcement corrosion, thereby restricting its direct use in reinforced concrete structures. However, the recent development of corrosion-resistant and non-metallic reinforcement materials has substantially mitigated this limitation. A typical seawater composition comprises approximately 55.1 % chloride ions, 30.6 % sodium ions, 2.3 % calcium ions, and 1.1 % potassium ions [17]. Meanwhile, except for chloride ions, the other three metal ions in SW can play a vital role in influencing the electrical resistance of cementitious composites [18]. Previous studies have shown that elevated alkali content reduces the resistivity of the pore solution owing to the increased concentration of dissolved alkali ions [19]. The potassium ion and sodium ion are introduced as alkali metal ions, and these ions can directly affect the ionic conductivity of the pore solution to reduce the electrical resistance of specimens [20]. Calcium ions also play a crucial role in governing the electrical conductivity of cementitious composites; however, unlike other metal ions, they influence conductivity through a distinct mechanism. Research has shown that the formation of calcium silicate hydrate (C–S–H) alters the pH of the pore solution, thereby affecting the overall ionic conduction within the matrix [21]. Furthermore, calcium ions can alter the microstructure of specimens, from the formation of hydration products, which refine the pore structure, and in turn, can affect the electrical conductivity of cementitious samples [22,23]. Self-sensing cementitious sensors can be embedded within concrete structures, and the incorporation of seawater in these sensors is not expected to significantly alter the ionic composition of the surrounding concrete's pore solution. In practical applications, the sensors are cast and cured separately, and the mature specimens are subsequently embedded into the structural elements to facilitate health monitoring and stress detection.

While most studies on CNT-cement composites, including those using MWCNTs, focus primarily on electrical percolation thresholds, the influence of ion conduction has rarely been considered. This study explicitly disentangles the contributions of MWCNT network percolation and ion conduction path, thereby bridging functional sensing performance with durability-related ion effects. Such positioning establishes a clearer framework for multifunctional cementitious composites in realistic SW-rich environments. From a materials perspective, Su et al. [24] indicated that SW enhances the early-age strength of cementitious composites, with an increase in the drying shrinkage of mortar bar specimens. After mixing with SW, the CO_2 uptake ability of $\beta - C_2S$ binder contributes to an increased strength of cement paste [25]. Moreover, the SW can lead to a reduced decomposition rate of $CaCO_3$, as well as the conversion of calcite to vaterite [26]. It has been proved that the combination of cementitious composites and SW can promote the mechanical properties of cement samples. The expected improved ionic conduction can also influence the piezoresistivity of self-sensing sensors [27]. This study aims to investigate the influence of seawater (SW) on the performance of self-sensing cementitious sensors, given that SW provides ions such as Na^+, K^+, and Ca^{2+} that may affect their electrical and microstructural properties. To ensure reliable and comprehensive results, a series of experimental techniques were employed, including electrical impedance testing, compressive strength testing, thermogravimetric analysis (TGA), X-ray diffraction (XRD), inductively coupled plasma (ICP) analysis, scanning electron microscopy (SEM), and energy-dispersive X-ray spectroscopy (EDS).

2. Materials and Methodologies

2.1. Raw materials

A General Purpose (GP) cement conforming to AS 3972 [28] was employed as the binder, while natural river sand served as the sole fine aggregate in the preparation of mortar specimens. The water-to-cement ratio was maintained at 0.4. Three types of mixing water were used: 100 % seawater (SW 100), a 50:50 mixture of seawater and tap water (SW 50), and 100 % tap water as the control (0SW). To enhance the self-sensing capability and electrical conductivity of the specimens, multi-walled carbon nanotubes (MWCNTs) were incorporated as the conductive filler [29]. In order to determine the percolation thresholds of the self-sensing sensors in the cementitious composites, the dosage rate of MWCNTs was varied at 0.1, 0.3, 0.5, 0.7, 1.0, 1.5, and 2.0 (wt% to cement) was applied in each specimen group. The details of components in each group are listed in Table 1.

A simulated seawater (SW) was prepared following the recommendations of ASTM D1141 [30], which is reflective of real ocean water [31]. The concentration of each component for SW preparation is listed in Table 2. To control the pH of the solution at a constant 8.2, an appropriate amount of NaOH was added to the SW. Table 3 shows the ion concentration of SW. As MWCNTs were utilised as the conductive filler in this study, the parameter of MWCNTs that has been used in this study was listed in Table 4.

2.2. Specimen preparation

The MWCNTs were first dispersed in deionised water or seawater (SW) using Triton X-100 as a surfactant, at a MWCNT-to-surfactant mass ratio of 1:2. Ultrasonic dispersion was conducted in an ultrasonic bath (40 kHz) for 40 min to achieve a homogeneous and stable suspension. Subsequently, the dry constituents, cement and sand, were mechanically blended in a 5 L Hobart mixer for 3 min to achieve uniform distribution. Depending on the specimen type, half of the mixing water or seawater (containing the pre-dispersed MWCNTs) was then introduced, followed by an additional 3 min of mixing. The remaining liquid was subsequently added and mixed for a further 2 min, resulting in a total mixing duration of 8 min. Throughout the process, the sides of the mixing bowl were periodically scraped to minimise material loss and ensure homogeneity.

The freshly prepared mixture was cast into 50 × 50 × 50 mm^3 cube moulds and vibrated for 3 min to remove entrapped air and ensure adequate compaction. The workability of the fresh mix was evaluated by the mini-slump test following AS 1012.3.5, with measured values ranging from 130 mm to 150 mm across all mixes, indicating consistent flowability. Copper mesh electrodes (40 × 75 mm) were embedded during casting, with 45 mm of each mesh inserted into the cement matrix and the remaining portion left exposed for wiring. The inner faces of the two electrodes were separated by 30 mm, which was used as the gauge length for electrical resistivity calculations. The same geometry was maintained across all mixes to ensure comparability. A schematic of the electrode configuration is provided in Fig. 1. Electrical characterisation was performed using a two-probe DC method under a fixed excitation voltage, with short measurement intervals to minimise electrode polarisation; selected samples were also verified by AC impedance spectroscopy.

The specimens were initially cured in the moulds for 24 h before demoulding and subsequently cured for 28 days in a controlled chamber at 95 ± 2 % relative humidity and 23 ± 2 °C. This consistent curing

Table 1
The components in each specimen group.

Specimen Type	CO	SW 50	SW 100
GP (g)	275	275	275
W/C	0.4	0.2	0
SW/C	0	0.2	0.4
M/C	0.1, 0.3, 0.5, 0.7, 1.0, 1.5, 2.0	0.1, 0.3, 0.5, 0.7, 1.0, 1.5, 2.0	0.1, 0.3, 0.5, 0.7, 1.0, 1.5, 2.0
S/C	1.5	1.5	1.5

Note: GP represent the General-Purpose cement, W/C is the water/cement mass ratio, SW/C is the seawater/cement mass ratio, M/C is the MWCNTs/cement mass ratio (wt%), S/C is the sand/cement mass ratio.

Table 2
Details of the components for simulated SW preparation.

Component	NaCl	$MgCl_2$	KCl	$CaCl_2$	Na_2SO_4
Concentration (g/L)	24.53	5.20	0.695	1.16	4.09

Table 3
Ion concentration of simulated SW (mmol/L).

Ions	Na^+	K^+	Ca^{2+}	Mg^{2+}	Cl^-	SO_4^{2-}
Concentration	484.3	10.5	10.6	54	565.5	29.2

Table 4
Parameters of Multi-Walled Carbon Nanotubes.

Purity	Inner Diameter	Outer Diameter	Length	Specific Surface Area	particle size
99 %	3–5 nm	8–15 nm	8–14 μm	≥ 250 m^2/g	< 25 μm

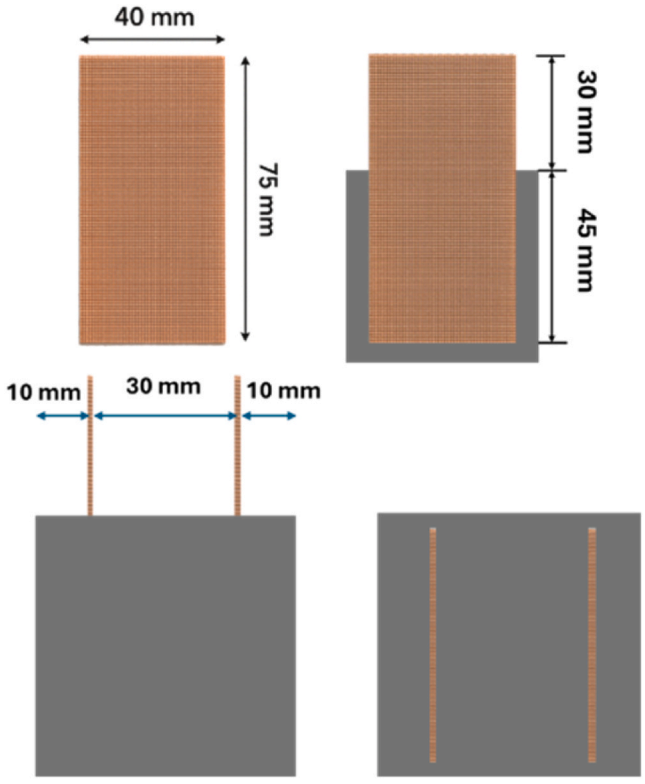

Fig. 1. The geometry and placement of electrodes.

regime minimised variations in moisture content, ensuring reliable assessment of seawater ion effects on the electrical and piezoresistive properties.

It should be noted that the incorporation of seawater inevitably increases the chloride concentration within the cementitious matrix. As the present study focuses on electrical and piezoresistive characteristics rather than reinforcement corrosion, direct corrosion analysis was not undertaken. For structural applications employing conventional steel reinforcement, appropriate corrosion mitigation strategies, such as epoxy-coated or stainless-steel bars, or corrosion inhibitors, would be essential. Conversely, when non-corrosive reinforcements (FRP or stainless steel) are used, the SW–MWCNT cementitious matrix can be employed without posing significant corrosion risks.

2.3. Methodologies

2.3.1. AC impedance spectroscopy (ACIS)

The ACIS test was applied to analyse the electrical properties of the specimens. A Solartron SI 1260 frequency response analyser, Zplot, and Zview programs provided support for sample testing and data analysis. The two probes measurement method was used, and the test protocols and reliability of this method are demonstrated in [32]. The cable was directly connected with the self-sensing specimens. The test frequency for specimens was between 1 Hz to 10 MHz.

2.3.2. Piezoresistivity test

To analyse the piezoresistivity performance of the specimens, compressive cyclic loads were applied to the specimens, and an electrical signal was collected by multimeters. The compression cyclic tests were conducted using an AGX 50 kN test machine under displacement-controlled loading. Each cementitious specimen was a cube with dimensions of 50 × 50 × 50 mm^3 , incorporating two embedded copper mesh electrodes (40 × 75 mm) for real-time electrical monitoring. The electrodes were positioned on opposing faces with a 30 mm gauge length between their inner surfaces.

The specimen was placed between two flat steel loading platens to ensure uniform stress distribution. A thin Teflon film was inserted between the specimen and platens to minimise frictional restraint and prevent electrode damage. Cyclic loading was applied between 0.235 kN (preload) and 10 kN (maximum load) at a loading/unloading rate of 1 kN/s, following four consecutive cycles. During each cycle, both mechanical stress–strain data and electrical resistance were synchronously recorded.

This setup enabled the evaluation of piezoresistive sensitivity, stability, and repeatability under varying compressive stresses. Each loading group consisted of four loading–unloading cycles. A direct current (DC) power supply of 10 V was used in the circuit, with a digital multimeter connected to the specimen for resistance measurement. DC power was selected for this study because, although alternating current (AC) can mitigate polarisation effects, it requires more complex instrumentation and sample preparation. Specifically, AC testing necessitates an impedance analyser and consideration of both inductive and capacitive components, whereas DC testing directly measures resistive behaviour, providing a simpler and more stable evaluation process [33]. The piezoresistivity test in this study is short-term (less than 3 min); as such, the DC setup can minimise the polarisation effect on the experimental results [34]. The fractional change of resistance (FCR) was measured by the following Eq. (1):

$$FCR = \frac{R - R_0}{R_0} \times 100\% \tag{1}$$

Where R represents the resistance after compression, and R_0 was the initial electrical resistance.

The percolation threshold was quantitatively determined from the resistance–dosage relationship using a derivative-based criterion. For each mixture, the discrete derivative of electrical resistance with respect to MWCNT dosage was calculated as Eq. (2):

$$\left|\frac{\Delta R}{\Delta p}\right| = \left|\frac{R_{i+1} - R_i}{p_{i+1} - p_i}\right| \tag{2}$$

where R is the measured electrical resistance and p is the MWCNT content (wt% of cement). The critical window was defined as the dosage interval showing the maximum $|\Delta R/\Delta p|$, corresponding to the sharpest drop in resistance and the initial formation of a continuous conductive network.

2.3.3. Early age hydration heat test

An isothermal calorimeter was used to measure the early-age heat of hydration. A TAM AIR THERMOSTAT facility was used to record the

heat evolved in the first 72 h of hydration, according to ASTM C1702 [35]. The heat evolved in the first hour of hydration was neglected because of the external temperature effect, and to allow the calorimeter to settle on a baseline.

2.3.4. X-Ray diffraction (XRD) test

XRD analysis was conducted to identify the crystalline phases present in the cement hydration products. After 28 days of curing, the cement pastes were ground into powder and dried in a controlled climate chamber at 35 °C for 5 days. Drying at 35 °C was selected to prevent thermal degradation of hydration products while ensuring sufficient removal of residual moisture for accurate phase identification. The scanning was 30 min long from 10° to 70° (2θ). The holder was filled with the powder and put into the Ultima IV diffractometer. The data was analysed using HighScore Plus software.

2.3.5. Thermogravimetric analysis (TGA)

A Thermogravimetric Analyser TA Instruments SDT 2960 was applied for assessment. TGA measurements were recorded to assess the mass loss of powdered specimens between 25 ℃ and 1000 ℃. The temperature rising rate was 10 K/min. To ensure the initial temperature started from 25 ℃, 5 min initial standby period was set before the test commenced. Derivative curve (DTC) was calculated by TGA results, and this curve was applied to identify phase loss in specific temperature ranges. The data was evaluated by the following Eq. (3) [36].

$$m_{CH} = \frac{M_{CH}}{M_H} \times m \tag{3}$$

Where M_{CH} represents the molar mass of portlandite (74.09 g/mol); m is the mass loss from the hydrated cement; M_H represents the molar mass of H_2O (18.02 g/mol); and m_{CH} is the cement mass fraction.

2.3.6. Micro-level structure analysis

A scanning electron microscope (SEM, Zeiss Supra 55VPP) was employed to examine the microstructural characteristics of hydrated cement pastes prepared with and without seawater (SW). To further elucidate the influence of SW on the hydration products, energy-dispersive X-ray spectroscopy (EDS) mapping and point analyses were performed to determine the elemental composition of the specimens after 28 days of curing. The samples were immersed in ethanol for 72 h to terminate hydration, then dried at 35 °C. Prior to observation, the specimens were further dried in a vacuum oven at 60 °C for 3 days to minimise charging and vacuum-induced damage during SEM operation. The accelerating voltage was set at 5 kV with a working distance of approximately 5 mm [37]. Then the specimens were contained in the vacuum containers to avoid the humidity influence.

2.3.7. Inductively coupled plasma (ICP)

An Inductively Coupled Plasma-Mass Spectrometry was used in this study. The influence of SW on the ion concentration of the pore solution of specimens, and consequently on the piezoresistivity of the self-sensing cementitious sensors, was investigated. After 28 days curing, the hardened pastes were ground into powder, and the powder was immersed in de-ionised water. To prevent the dilution effect, the powder to water ratio was maintained at 1:5. The centrifugation at 5000 rpm for 20 min was employed to collect the supernatant, after 48 h of immersion [38]. The target ions in this study were Na^+, K^+, Ca^{2+}, Fe^{2+}, and Mg^{2+}.

2.3.8. Compression test

The 28-days compressive strength of the cementitious specimens (CO, SW 50, and SW 100) was measured using a UH 500 kN compression machine. A compressive stress was applied on the 50 × 50 mm^2 surface until failure. Data gathered was reflective of the influence of SW on the mechanical properties of the cementitious composites.

2.3.9. Water absorption

Water absorption tests were conducted to evaluate the relative pore content of specimens prepared with and without SW, in accordance with AS 2983.18. After 28 days of curing, the specimens were submerged in water until a constant mass was achieved, indicating full saturation. Subsequently, the samples were oven-dried at 105 °C until a constant mass was again attained to determine the absorbed water content. This mass was recorded as M_1 (dry mass). Then, the specimens were immersed in water again for three days until fully saturated. The mass of the samples measured was recorded as M_2 (saturated mass). Before measuring the saturated mass, extra surface water was eliminated using cotton cloth. The water absorption rate (R) was calculated using Eq. (4):

$$R = \frac{M_2 - M_1}{M_1} \times 100\% \tag{4}$$

3. Results and discussion

3.1. Early hydration heat

The heat flow and cumulative heat results presented in Figs. 2 and 3 demonstrate that SW enhances the hydration process of cement. Both SW 50 and SW 100 exhibited higher peak heat flow values (0.184 W/g and 0.187 W/g, respectively) compared with the 0 SW mix. The SW 100 specimen reached its peak at approximately 6.6 h, while SW 50 reached a similar peak at 6.7 h, around 3 h earlier than the 0 SW specimen, indicating a markedly accelerated hydration reaction. The 0 SW mix displayed a lower peak heat flow of 0.132 W/g, approximately 28.8 % below that of the SW specimens. As shown in Fig. 3, the SW 50 mix exhibited the highest cumulative heat release (261 J/g) after 72 h of hydration, followed by SW 100 (250.48 J/g), representing 14.24 % and 9.63 % increases, respectively, compared with 0 SW. These findings confirm that the inclusion of SW promotes higher heat evolution and accelerates the early-age hydration of cementitious materials. The chloride ions of SW promote cement hydration, also supported by Qu et al. [39]. This is a consequence of a greater number of ions like Cl^{-1}, SO^{-2}, and Na^+ dissolved in SW, performing as the catalyst to accelerated the hydration process of alite (C_3S) [40]. Furthermore, there are several Ca^{2+} ions dissolved in the SW, contributing to the formation of additional hydration products [41].

3.2. XRD experimental results

Fig. 4 shows the XRD test results of the paste portion of the 0SW, 50

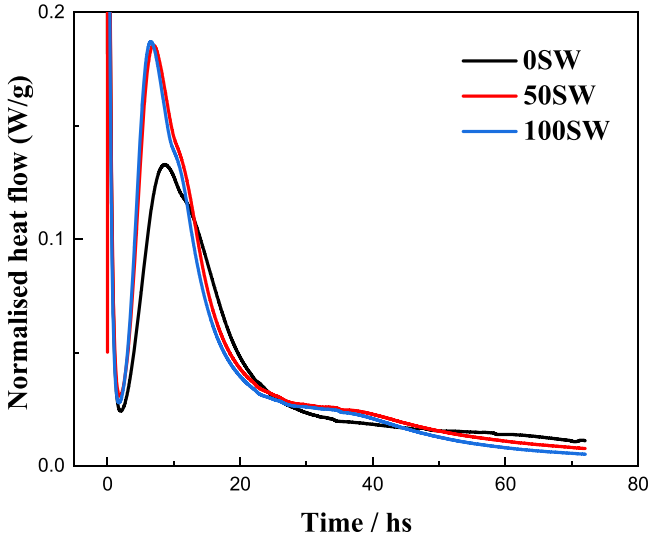

Fig. 2. The IC test results of early hydration heat release flow curve in 72 h.

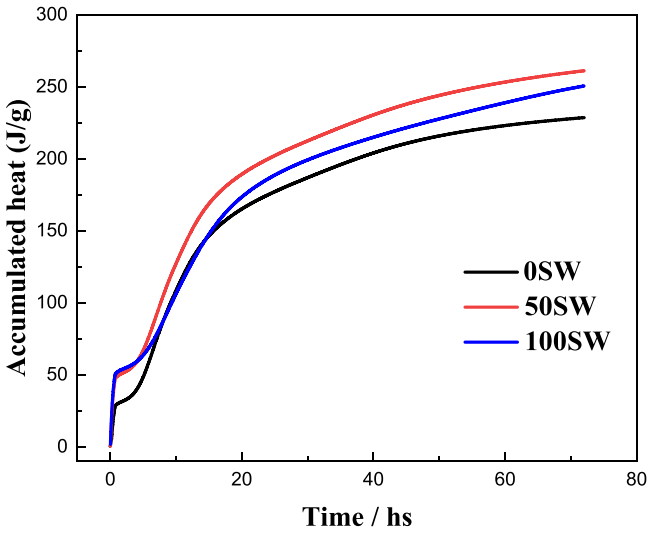

Fig. 3. Accumulated heat of three types of specimens in 72 h.

SW, and 100 SW specimens after 28 days of curing. The primary phases of cementitious specimens including, C_3S (32.1º and 41.2º), C_2S (32.5º), calcium silicate hydrate (31º), portlandite (18º), ettringite (9.1º, 15.8º, and 23º), and calcite (23.1º), can be identified in Fig. 4. The C_3S and C_2S reflect the unhydrated particles, while the rest of the compounds are cement hydration products. Quartz can also be observed in Fig. 4 (20.8º, 23.9º, 26.7º, 29.4º, 36.4º, and 42.4º). In addition to these expected phases in the hydrated cementitious matrix, additional products can also be identified. Friedel's salt can be detected predominantly in the SW samples located at 12º, 23º, and 39.3º. Compared to the 0SW specimen, the peaks at these locations for 50 SW and 100 SW were higher. The occurrence of Fridel's salt is related to the chloride content of SW. Moreover, the peaks at 9.1º, 15.8º, and 23º, indicating ettringite, do not present obvious differences between the samples. This indicates that SW does not affect the formation of ettringite. However, the formation of hydrotalcite (12º, 23º, and 35.8º) is observed, particularly in the SW samples, from the presence of magnesium and sulfate. Also, SW led to the formation of monosulfate (11.3º, 30.3º, and 35.1º) due to the presence of sulfate ions in the SW [42]. Brucite identified at 18.6º, 38º, and 50.9º are not as pronounced due to the low content of available magnesium in SW; the magnesium is consumed in the formation of hydrotalcite and monosulfate. In summary, SW can affect the phases in cementitious composites, particularly by forming additional reaction products compared to the 0SW specimen. These additional products that may reduce the water of the specimens. These products resulted in a higher heat of hydration and are also expected to improve the compressive strength of SW specimens.

3.3. TGA and compression test results

The TGA results are shown in Fig. 5. The common hydration products can be detected, and the three major peaks can be observed from the DTG results. The mass loss in the range of 50–200 ℃ is from the evaporation of free water, the bond water on the Friedel's salt, and the decomposition of C-S-H in the specimens. The second peak observed between 400 ℃ and 500 ℃ is related to the decomposition of portlandite/$Ca(OH)_2$. The third peak occurred between 600 ℃ and 750 ℃, resulting from the decomposition of calcite [43]. Compared to the 0SW specimens, the mass loss between 450 ℃ and 500 ℃ was greater in 50 SW and 100 SW specimens. The mass loss of 50 SW within this temperature range is 1.38 % compared to 1.19 % in the 0SW samples. The extra mass loss in this temperature range can be related to the loss of coordinated water in magnesium silicate hydrate (MSH) gel and the decomposition of MSH [44]. The formation of MSH is related to the free Mg^{2+} in SW, but undetected in the XRD analysis because of its poorly crystalline nature. Also, due to the low content of magnesium ions, the mass loss gap between specimens with/without SW is not obvious. The mass loss between 600 ℃ and 750 ℃ of 50 SW and 100 SW specimens reached 2.5 % and 2.7 %, respectively, which are comparatively higher than that of the 0SW samples (2.3 %). Although minor in magnitude, this additional mass loss may be related to the decomposition of $MgCO_3$ [45,46].

The compressive strength of specimens with/without SW has been tested, and the results are shown in Fig. 6. The corresponding standard deviations were between 0.8 MPa and 1.4 MPa, confirming the good repeatability of the mixing and testing procedures. It can be observed that with 100 % SW, the compressive strength of specimens reached

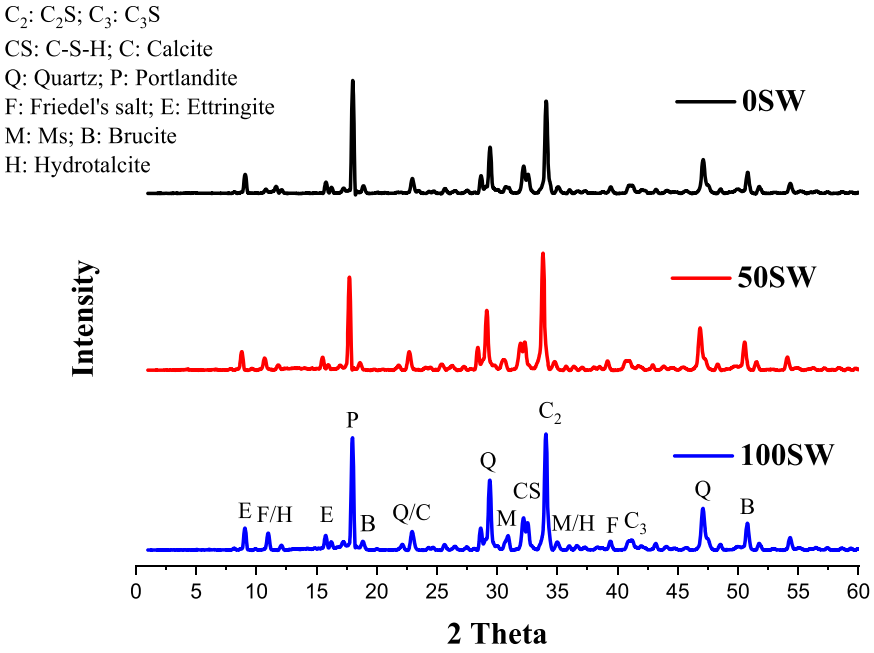

Fig. 4. XRD results of three types of specimens after 28 days curing.

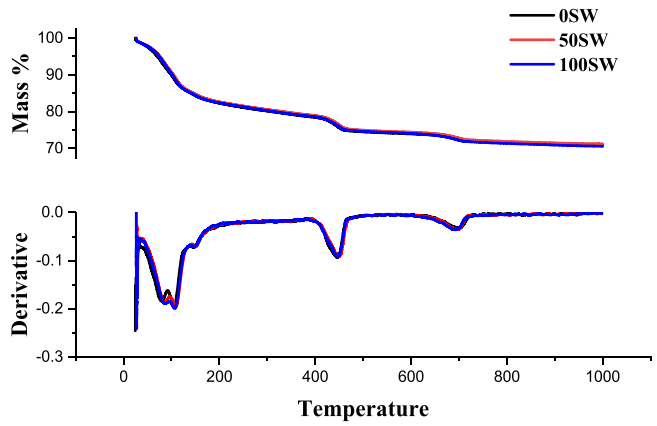

Fig. 5. TGA test results of 0SW, 50SW, and 100 SW specimens after 28 days curing.

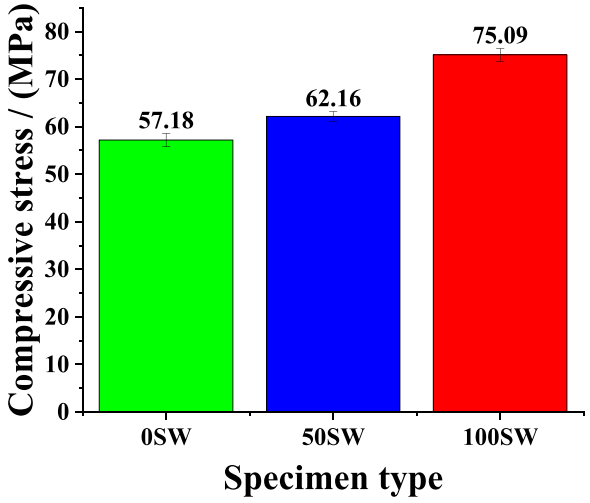

Fig. 6. Compressive strength test results of 0SW, 50SW, and 100SW specimens.

75.09 MPa, the highest of the cases investigated, followed by 50 SW, with a compressive strength of 62.16 MPa. The 0SW samples reached 57.18 MPa, 8.71 % and 31.32 % lower than the 50 SW and 100 SW. As identified in XRD and TGA analyses, the SW can improve the hydration of cementitious samples. This is reflected in the compressive strength of the samples. The influence caused by SW was mainly due to the chloride and sulphate ions, forming additional reaction products, as identified in XRD and TGA [39].

3.4. Percolation thresholds of self-sensing cement sensors

To identify the percolation thresholds of the different self-sensing specimens, electrical impedance spectroscopy was conducted, and the representative results for the 50 SW mixture are presented in Fig. 7. In the impedance plot, the horizontal axis corresponds to the real component (electrical resistance) of the self-sensing cementitious matrix, while the vertical axis represents the imaginary component (electrical reactance) of the specimens. The leftmost point along the X-axis indicates the intrinsic resistance of the material. This method enables the differentiation and quantification of the resistive and reactive contributions of various components within the composite mixture [47]. Moreover, compared to DC resistance test (multimeter), the AC power with a range of frequency allow the deep analysis of materials and can avoid the polarisation effect of semi-conductors [48]. With the help of electrical impedance test, the percolation thresholds were presented in Fig. 8.

The percolation thresholds were the suitable working range of self-

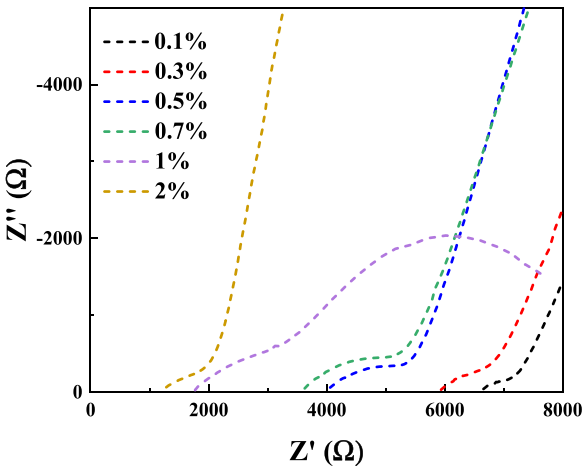

Fig. 7. Electrical impedance test results (50 SW, representative of the rest).

sensing specimens. The piezoresistivity of self-sensing cementitious matrix can present the highest fractional change of resistance (FCR) value and specimens performs the most sensitivity to the loading change that applied on the surface of sensors [49]. Based on derivative-based criterion, a common critical window at 0.3–0.5 wt%, where resistance dropped most sharply for all mixtures. The 50SW specimens exhibited the highest slope magnitude (7.1×10^5 Ω / wt%), indicating the most distinct percolation transition.

According to experimental results, with 100 % SW mixed in the mixture, the electrical resistance of each specimen has increased. That was resulted to the chloride ions can be absorbed by C-S-H gels which reduce the volume of macro pores in cement matrix [50]. The curve of 100SW percolation thresholds was higher than the 0SW samples. Furthermore, the range of the percolation thresholds become narrow. For 0SW specimens, the upper side of thresholds was the specimen with 0.3 wt% MWCNTs while the lower side of thresholds was samples with 1 wt%. Although the upper side of thresholds of 100SW specimens kept same, the lower side of percolation thresholds was mixtures with 0.7 wt %, as the slope of the curve changed immediately after this point.

Compared to 0SW specimens, the range of the percolation thresholds of 50SW keeps the same (ranged from 0.3 wt% to 1.0 wt% MWCNTs). However, the thresholds of 50SW cover a larger range of electrical resistance and a steeper slope of the curve can be observed. The major factor that influences the electrical resistance of specimens was Na^+, K^+, and Ca^{2+} ions which has been indicated by the previous study [51].

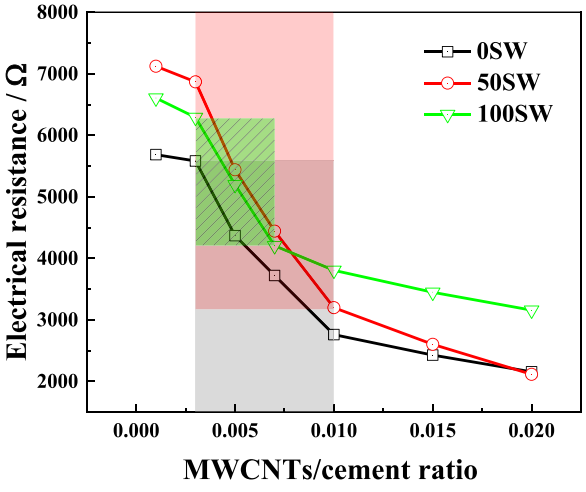

Fig. 8. Percolation thresholds of three types of self-sensing cementitious sensors.

Although classical percolation theory is often expressed as $\sigma = A(p - pc)^t$, the limited number of MWCNT dosages tested near the threshold (0.3–1.0 wt%) prevented reliable nonlinear fitting of pc and t. Instead, the onset of conductivity increase was used to qualitatively identify the percolation threshold range. That may also influence the piezoresistivity of specimens. Further explanation will be introduced in Section 3.6.

3.5. Piezoresistivity performance

The piezoresistivity performance of the self-sensing sensors at 0.5 % and 0.7 % MWCNTs dose was evaluated using electrical response in terms of FCR as per Eq. (1) and illustrated in Fig. 9, when specimens went through a cyclic loading and unloading. The electrical resistance, i.e., the FCR, changed in a pattern analogous to the loading and unloading applied to the specimen. This phenomenon was due to the volume change of pores under compression, leading to the formation of new conductive paths [52].

Based on the self-sensing results in Fig. 9, compared to 0SW specimens, the sensitivity of SW specimens to the change in loading was greater, as marked by the greater fluctuations of FCR. Also, this sensitivity is more pronounced for specimens with 0.7 % MWCNTs compared to 0.5 %. For 0.5 wt%, the FCR in 0SW specimens reached up to 0.035 %, while the same for 100 SW specimens reached up to 0.065 %. The 50 SW specimens with 0.5 wt% conductive filler performed the best, as indicated by the FCR value of around 0.100 %. A similar trend is also observed when the MWCNTs dose was increased to 0.7 %. At 0.7 wt% MWCNTs in the specimens, the FCR of 0SW samples was about 0.070 %, but it improved to 0.14 % for 100 SW specimens. Similar to 0.5 % MWCNTs, for the 0.7 % MWCNTs, the 50 SW specimens reached the highest FCR value of 0.225 %.

Analysis of the FCR indicates that, in addition to the conductive fillers forming percolated networks, the ions present in the pore solution of SW specimens also contribute to the development of supplementary conductive pathways during loading. However, comparison between the 100 SW and 50 SW specimens reveals that excessively high ionic

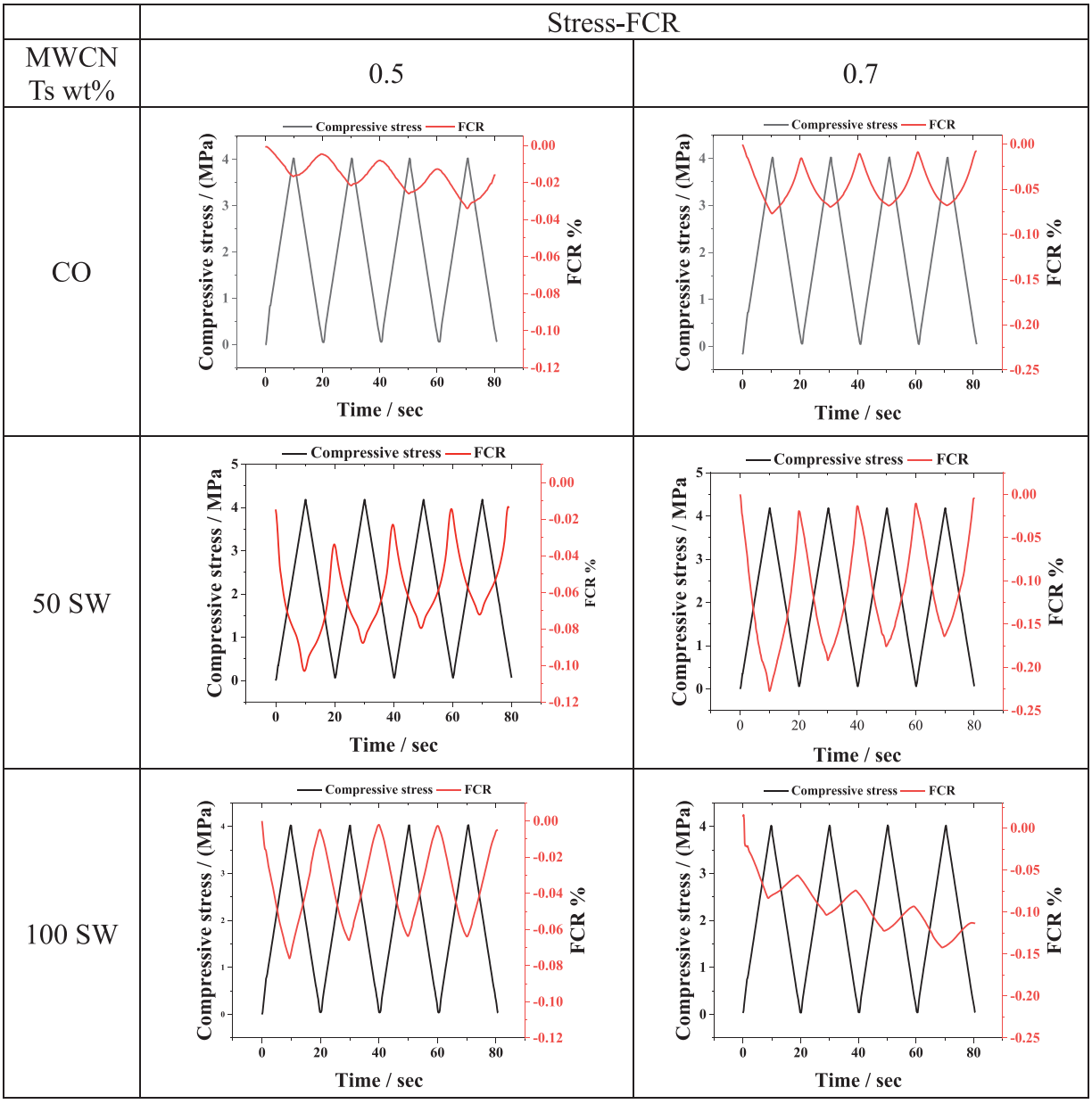

Fig. 9. Compressive stress and FCR relationship of three types of self-sensing cementitious sensors.

concentrations can diminish the FCR response. As shown in Fig. 9, the 50 SW specimens exhibited a higher FCR than the 100 SW specimens, reflecting differences in electrical resistance behaviour. When the ion concentration is elevated, as in 100 SW, the electrical resistance under zero load is inherently lower due to the abundance of pre-existing conductive paths. Upon loading, however, fewer new conductive bridges are formed compared with 50 SW, as confirmed by the lower FCR values. This suggests that surplus ions no longer enhance piezoresistivity once the optimum ionic threshold is exceeded. The results therefore indicate that a balanced combination of MWCNT content and ion concentration is essential to achieve optimum self-sensing performance.

Comparison between mixes with and without SW further supports this conclusion. The initial conductivity of 50 SW and 100 SW specimens was higher than that of 0 SW specimens, owing to the presence of free ions in the pore solution. During cyclic loading, the formation of additional conductive paths was more pronounced in SW-containing mixes, resulting in greater FCR variation. Consequently, the incorporation of SW enhances the piezoresistive sensitivity of cementitious sensors through both ionic conduction and filler-induced network formation.

3.6. Microstructure of self-sensing specimens

The morphology of the multi-walled carbon nanotubes (MWCNTs) within the self-sensing cementitious specimens, as observed by SEM, is presented in Fig. 10(a), while the corresponding EDS elemental quantification is shown in Fig. 10(b). As illustrated in Fig. 10(a), the nanotubes are well dispersed within the cement matrix, and the EDS analysis confirms a carbon content of approximately 67.4 % in the analysed region. This dominant carbon presence verifies the uniform distribution of conductive fillers. Furthermore, Fig. 10(a) reveals that the MWCNTs are interconnected, forming a continuous conductive network that enhances the specimen's electrical conductivity even in the absence of external loading. The EDS elemental mapping results in Fig. 11 further support these findings, showing the expected presence of Si, Ca, and Al, along with trace amounts off Cl. Notably, the widespread distribution of carbon throughout the specimen confirms the effective dispersion and integration of MWCNTs within the cementitious matrix.

In Fig. 12, Friedel's salt was identified with EDS, originating from the use of SW, and point scans were undertaken for confirmation. It can be detected in Fig. 12(a), marked by the cubic morphology and plate-like crystals [53]. With the increase of chloride ions, the plate-like Friedel's salt structure can be more prominent in SEM images [54]. The formula of Friedel's salt is $Ca_4Al_2Cl_2(OH)_{12} \bullet 4H_2O$, indicated by the existence of chlorine, aluminium, calcium, and oxygen in Fig. 12 (b-d). The XRD, SEM, and EDS analyses strongly indicate the existence of Friedel's salt in SW specimens.

Representative SEM micrographs obtained at 20,000 × to 40,000 × magnifications are shown in Fig. 13. The plate-like layered structures correspond to Friedel's salt, confirming chloride incorporation and binding within the matrix. The formation of Friedel's salt in seawater-mixed specimens also indicates that chloride ions were chemically bound, thereby reducing their free concentration in the pore solution.

3.7. ICP ion concentration test results

Ion concentration in the pore solution is vital in influencing the electrical resistance of cementitious specimens. Ions like Na^+, K^+, Ca^{2+}, Fe^{2+}, and Mg^{2+} has been analysed in this study and the ICP test results are shown in Fig. 14. The ICP results confirmed that Na^+, K^+, and Ca^{2+} ions were the dominant species influencing the electrical conductivity of the SW-mixed MWCNT–cement composites. The measured ionic concentrations were in good agreement with those reported for SW-cement systems in previous studies [51,55]. In particular, Na^+ and K^+ ions, which remain largely unbound in the pore solution, contribute strongly to the ionic component of conductivity, whereas Ca^{2+} is partially incorporated into hydration products such as C–S–H and Friedel's salt, thereby reducing its free-ion concentration. The slightly higher K^+ and Na^+ concentrations (in SW mixed specimens) observed in this study can be attributed to the high ion strength of the artificial SW used and to partial chloride fixation within the matrix. These trends align with previous findings that the balance between bound and free cations governs both electrical conductivity and the degree of chloride immobilisation in seawater-based cementitious systems.

According to Table 2, elements like NaCl, $MgCl_2$, KCl, and $CaCl_2$ were added in the SW specimens, to simulate seawater. The GP cement used as the binder also contains traces of K_2O, Fe_2O_3, and Na_2O [51]. Considering the ions present in SW and the cement, the aforementioned five metal ions have been analysed in this study. Compared to 0SW specimens, there is a significant difference between the sodium ion concentration in specimens with/without SW. Because of the high amount of dissolved sodium ion in SW, the free Na^+ in pore solution can be detected at a high concentration. The Ca^{2+} ion concentration was consistent between the three types of specimens. This may be due to the absorption of free Ca^{2+} during the hydration process and observed in the TGA results. With higher mass loss in the temperature range between 600 ℃ to 800 ℃, hydration products containing Ca^{2+} is higher in the SW specimens compared to the control group. This is also reflected in the compressive strength measurements.

As the piezoresistivity is influenced significantly by Na^+, K^+, and

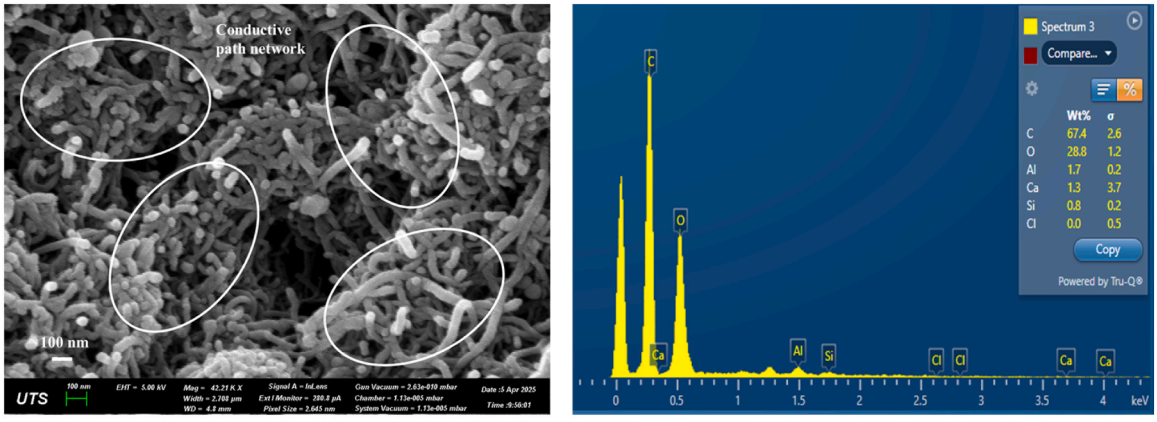

Fig. 10. (a) MWCNTs morphology in self-sensing cementitious specimens and (b) EDS map scan results of MWCNTS.

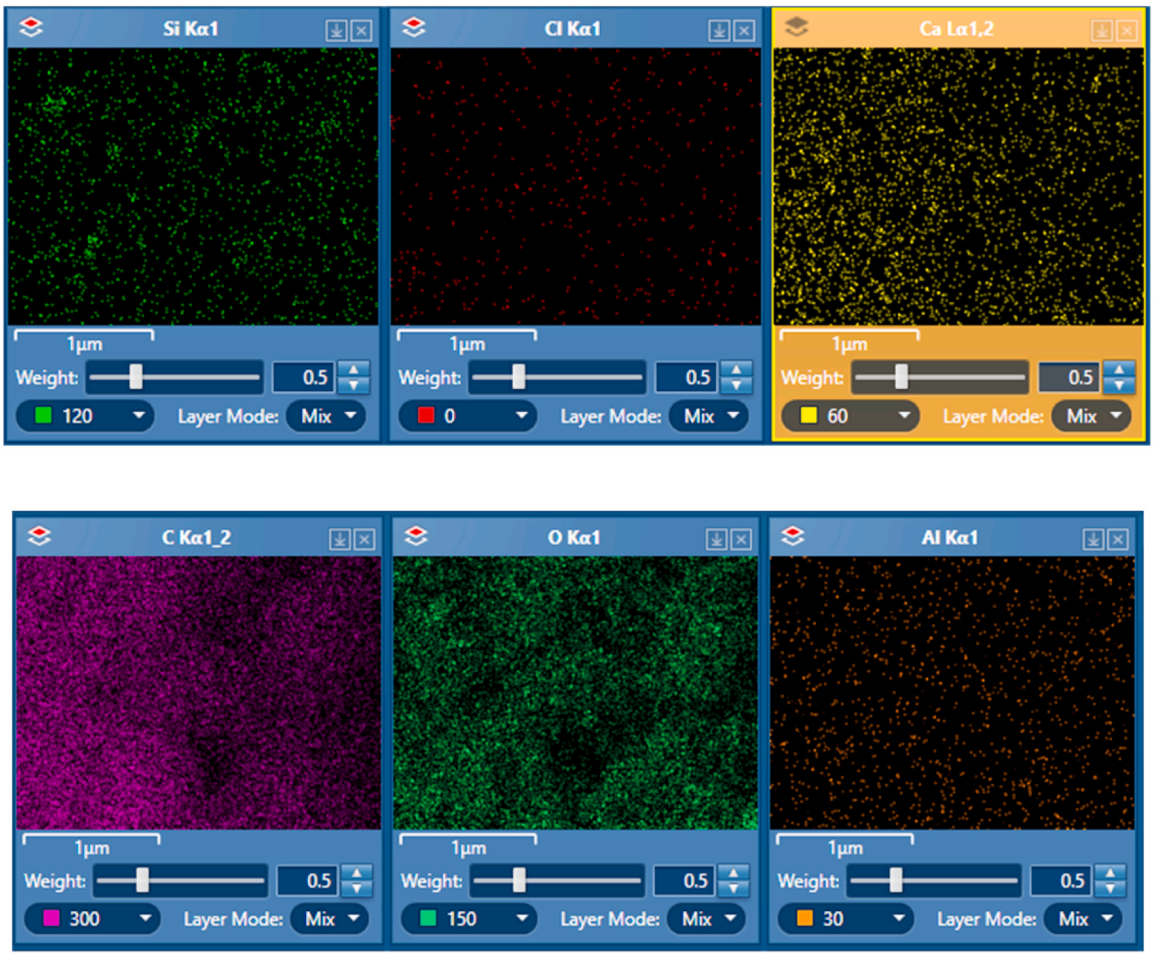

Fig. 11. The EDS map scan of MWCNTs in self-sensing cementitious specimens.

Ca^{2+} ions, they have been measured separately in this study. There is a strong relationship between electrical resistance and ion concentration in the pore solution [27]. The differences in the ion concentration are shown in Fig. 14. It is worth noticing that the high concentrations of those three ions can reduce the electrical resistance of the specimens, leading to low piezoresistivity, as confirmed in this study and in the literature [56]. On the other hand, the high amount of dissolved chloride ions in the SW enhances the hydration of cement, leading to reduced pore volume and increased density of specimens. While free ions lead to better conductivity, free chloride densifies the microstructure to improve resistivity. Both of these phenomena influence the electrical resistance of self-sensing sensors. This may explain the relatively better piezoresistivity performance of 50 SW specimens compared to 0 SW and 100 SW.

3.8. Discussion of ion concentration influence on piezoresistive performance

It should be noted that the MWCNTs incorporated in this study are chemically inert and do not directly participate in the hydration reactions of cement. Instead, their influence is primarily physical and interfacial. The oxygen-containing surface groups (–OH, –COOH) on the MWCNTs can adsorb Ca^{2+} and $Si(OH)_4$ species, serving as heterogeneous nucleation sites for the growth of hydration products such as C–S–H and ettringite [57,58]. Additionally, these polar surface groups can form hydrogen bonds with water molecules, improving local moisture retention and facilitating continuous hydration near the nanotube surfaces. Through these mechanisms, MWCNTs promote a denser microstructure and enhance ionic conduction pathways, thereby improving electrical sensitivity without chemically altering the cement phases [59].

The incorporation of SW influences the self-sensing performance of cementitious composites through several interrelated mechanisms. The concentration of free ions in the pore solution increases with higher SW content, enhancing ionic conduction within the matrix. Calorimetry results indicate that SW accelerates the early-age hydration process, leading to greater heat evolution. Complementary XRD and TGA analyses confirm the formation of additional hydration products, such as Friedel's salt, alongside conventional phases, thereby contributing to the increased compressive strength observed in SW specimens. This enhancement is further supported by the reduced water absorption shown in Fig. 15, suggesting a denser pore structure induced by the presence of chloride ions. In addition to promoting Friedel's salt formation, chloride ions may also be incorporated into the C–S–H structure during hydration, effectively reducing pore volume and improving the compactness of the cement matrix [60]. Consequently, the SW not only improves the compressive strength of the specimens from a decrease in the pore volume, but it also increases the electrical resistance of self-sensing specimens. It can be observed from the percolation thresholds of specimens (in Fig. 8), the electrical resistance of both 50SW and 100SW was higher than the CO samples.

ICP analysis (Fig. 14) confirmed that Na^+, K^+, and Ca^{2+} were present at the highest concentrations in the pore solution, whereas Mg^{2+} and SO_4^{2-} were comparatively lower. The predominance of Na^+, K^+, and Ca^{2+} indicates that these cations provide the dominant ionic conduction pathways that reduce the resistive component of the impedance spectra.

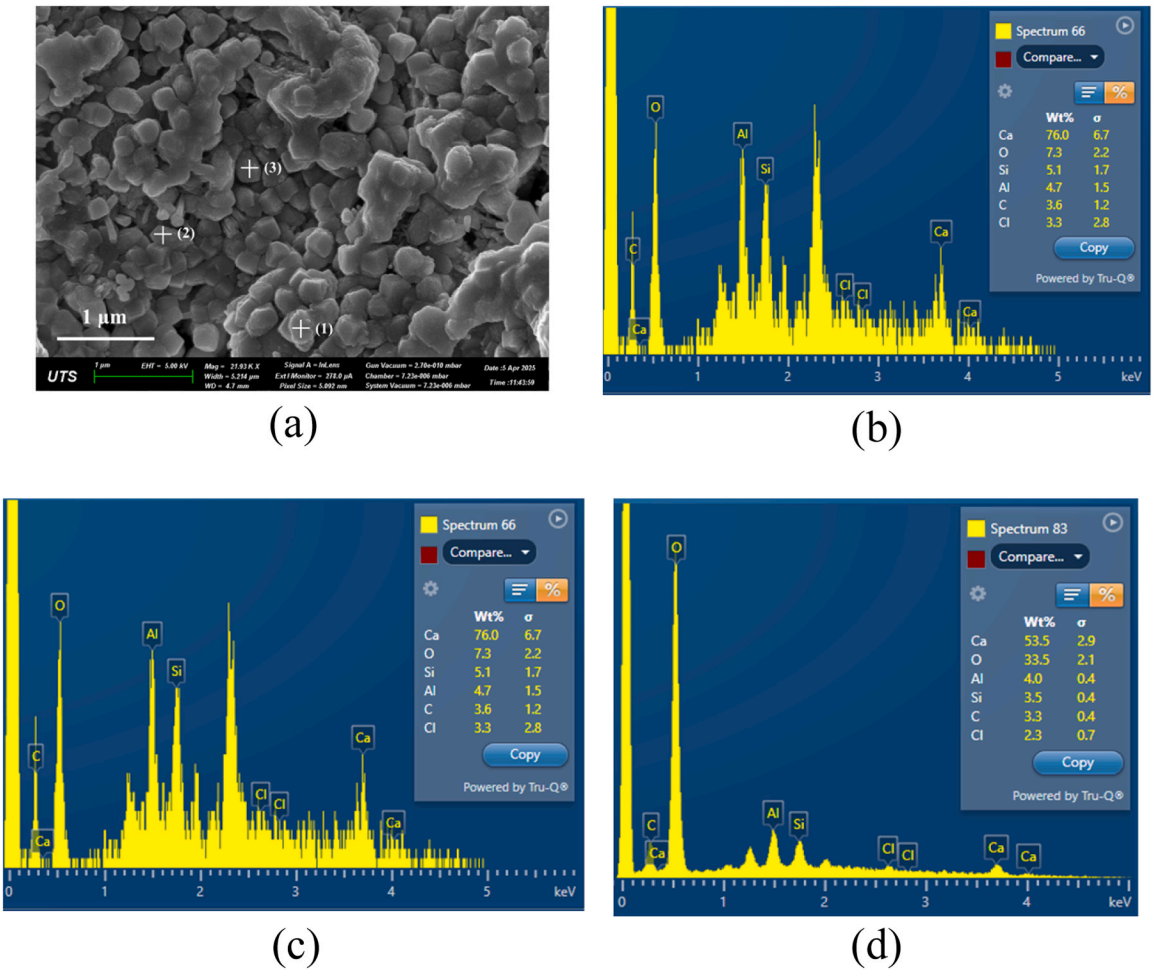

Fig. 12. (a) SEM image of the morphology of Friedel's salt; (b) EDS point scan of point 1 in figure (a); (c) EDS point scan of point 2 in figure (a); (d) EDS point scan of point 3 in figure (a).

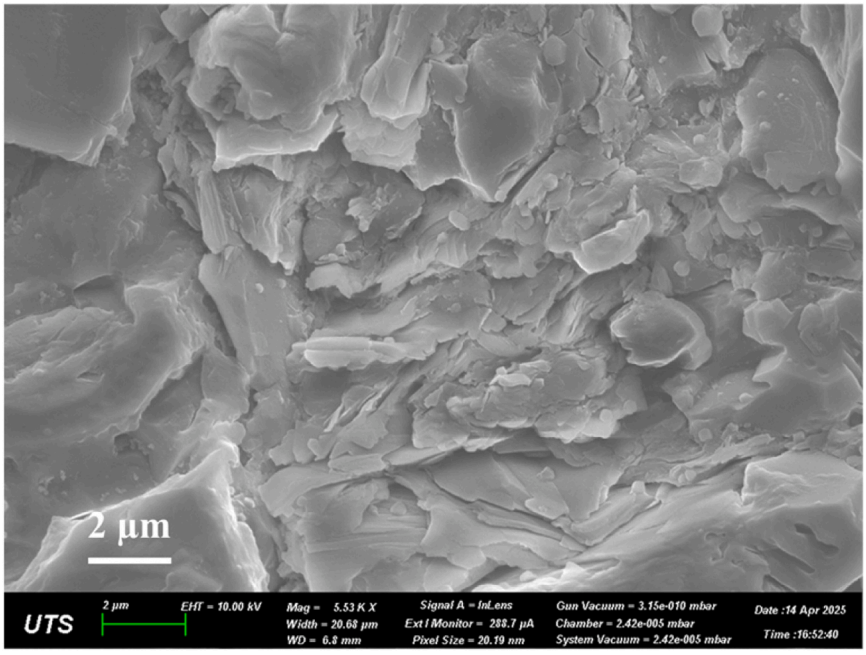

Fig. 13. Representative SEM micrographs of the cementitious composites at high magnification: Plate-like Friedel's salt observed in seawater-mixed specimens, showing the layered morphology typical of chloride-binding phases.

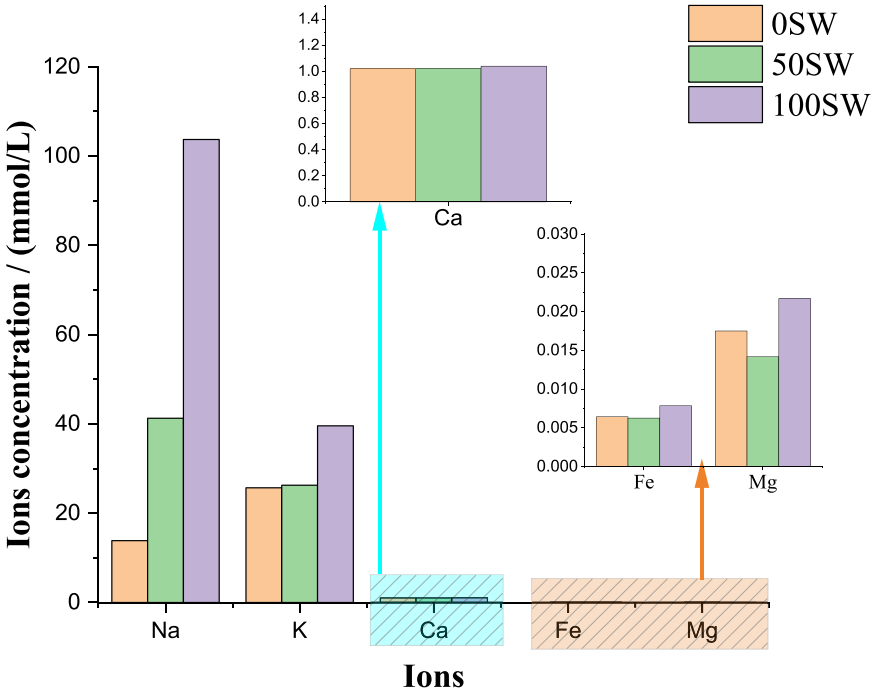

Fig. 14. The ion concentration of five metal ions in the pore solution.

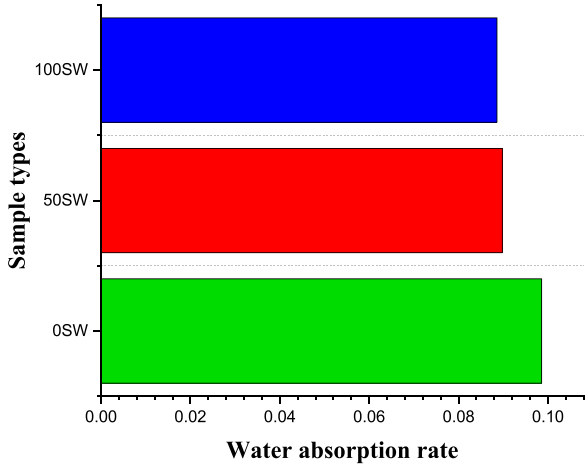

Fig. 15. The water absorption rate of three types of specimens.

This outcome aligns with the observations of [51], who emphasised the decisive role of Na^+, K^+, and Ca^{2+} in controlling the electrical resistance of cementitious composites. In contrast, the contribution of SO_4^{2-} and Mg^{2+} ions were minimal, which explains why these species were not considered in the impedance fitting and interpretation. The combination of MWCNT electronic pathways with Na^+, K^+, and Ca^{2+} driven ion transport offers a more accurate representation of the conductivity mechanisms in SW-mixed systems. A summary of key performance indicators for all mixtures is presented in Table 5. The results reveal that the 50SW mixture exhibited the highest compressive strength and FCR values, indicating an optimal balance between ionic conductivity and microstructural densification. In contrast, the 100SW composite showed reduced FCR and slightly lower strength, likely due to excessive ionic content hindering the formation of new conductive paths under load.

In the seawater-mixed MWCNT cementitious composites, the electrical transport process arises from the cooperation between ion and electron conduction rather than from two independent pathways. The electronic conduction provided by the MWCNT network establishes a

Table 5
Summary of the key findings.

	0SW	50SW	100SW
28 days compressive strength / MPa	57.18	62.16	75.09
Water absorption rate	0.0986	0.0898	0.0886
Na^+ concentration / mmol/L	13.85	41.25	103.72
K^+ concentration / mmol/L	25.69	26.27	39.56
Ca^{2+} concentration / mmol/L	1.02	1.02	1.04
FCR % 0.5 % MWCNTs	0.035	0.100	0.065

continuous backbone for charge transport, while the ion conduction, mainly contributed by Na^+, K^+, and Ca^{2+} ions dissolved in the pore solution, enhances interfacial charge transfer and improves network connectivity. The ionic species can form local conductive bridges across partially separated nanotubes, reducing contact resistance and stabilising the electron transport process. Consequently, the total electrical conductivity and piezoresistive response reflect the combined and interactive contributions of these two mechanisms. Similar cooperative effects have been reported in carbon-based cementitious sensors [59, 61], confirming that ion mobility can assist electron tunnelling and improve the reproducibility of sensing performance.

According to the piezoresistivity results (Figs. 8 and 9), the sensitivity of the specimens to load change is enhanced by high ion concentrations, and the pure value of FCR also improves. The results prove that more conductive paths can be formed with the addition of SW to the specimens. Fig. 15 illustrates the schematics of the phenomenon, describing the influence of SW on self-sensing performance. First, with chloride ions in the SW forming additional hydration products, the volume of pores decreases [46]. With smaller pores, at a constant conductive filler content, the less conductive path can be formed under the initial status (zero loading), compared to the 0SW specimens. In 50 SW specimens, higher ion concentration can be observed in Fig. 15. With the increase of conductive filler content, compared to 0SW specimens, more conductive paths can be formed due to the ion conduction influence. Because of that, the electrical resistance gap between 0.1 wt% MWCNTs 50 SW specimens and 1.0 wt% MWCNTs 50 SW specimens was wider than the 0SW specimens. As mentioned above, this ion

conduction also enhanced the slope of the percolation threshold curves. With high ion concentration and low pore volume in self-sensing specimens, the initial electrical resistance of specimens was decreased (compared between 50 SW and 100 SW). Then, with the help of additional ions, new conductive paths were formed under the initial status, due to the higher ion concentration (compared between 50 SW and 100 SW specimens). As illustrated in Fig. 16 (b), the piezoresistive response is governed by the cooperative interaction between ionic conduction in the pore solution and electronic conduction through the MWCNT network. When the seawater ratio is low (0SW), insufficient ions limit charge transfer despite MWCNT deformation. At high salinity (100SW), abundant ions reduce initial resistance but screen MWCNT–MWCNT contacts, suppressing the formation of new conductive paths under load. In conclusion, the 50SW mixtures provide an optimal balance, maintaining adequate ionic mobility to assist charge transfer while preserving the network's mechanical sensitivity, resulting in the highest FCR values.

Although this study concentrates on the mechanical and sensing performance of MWCNT–cement composites mixed with seawater, the long-term durability implications of chloride ingress should be considered for reinforced applications. The incorporation of seawater increases the free chloride content in the pore solution, which may accelerate corrosion of conventional carbon-steel reinforcement under cyclic wet–dry or marine exposure conditions [62,63]. However, the formation of Friedel's salt and other chloride-binding phases within the matrix can partially immobilise chloride ions, reducing their mobility [64]. For structural applications, mitigation strategies such as the use of stainless-steel or FRP reinforcement, epoxy-coated bars, or corrosion inhibitors are recommended. The findings presented here remain directly applicable to systems with non-corrosive reinforcement or to unreinforced sensing and surface-layer applications, where chloride-induced corrosion is not a governing concern.

4. Conclusion

This study investigated the mechanical and piezoresistivity of cementitious specimens under the influence of SW. The use of SW in cementitious composites enhances piezoresistivity and compressive strength. The combination of mechanical, electrical, and microstructural analyses in this study provides a comprehensive understanding of the multifunctional performance of MWCNT–cement composites. The integration of macroscopic strength evaluation, microscopic phase characterisation, and conductivity measurements allows a unified interpretation of how seawater ions and carbon nanotube networks jointly influence the mechanical and sensing behaviour of the material. The major conclusions of the systematic analyses undertaken in this study are as follows:

1. The incorporation of seawater (SW) enhanced the hydration process of the self-sensing cementitious specimens, resulting in increased compressive strength after 28 days of curing. The presence of SW also promoted the formation of additional hydration products, such as Friedel's salt, contributing to the densification of the microstructure and the overall improvement in mechanical performance.

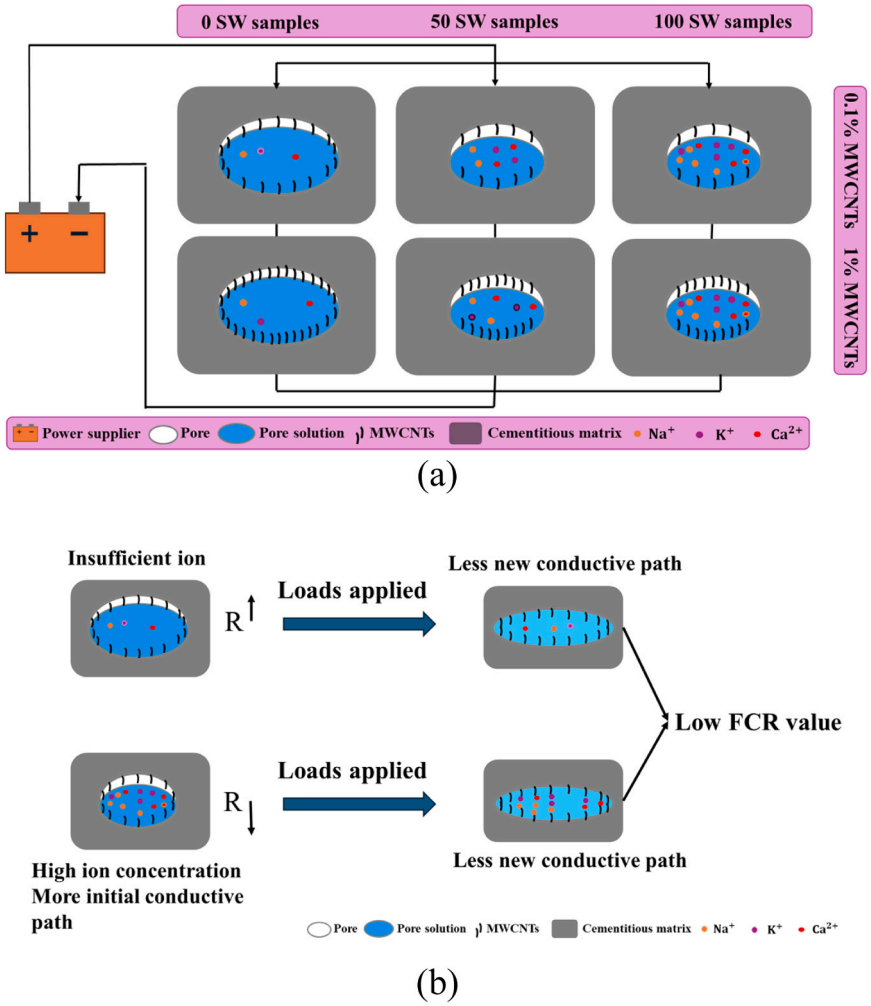

Fig. 16. Explanation of ion conduction influence on (a) initial electrical resistance, and (b) piezoresistive performance of self-sensing specimens.

2. Ion conduction plays a crucial role in determining the percolation threshold of self-sensing cementitious sensors. In this study, the mixture containing a 50/50 blend of seawater and tap water (SW 50) exhibited the steepest percolation curve, indicating enhanced electrical connectivity. The corresponding ion concentrations in the pore solution were 41.25 mmol/L for Na^+, 26.27 mmol/L for K^+, and 1.02 mmol/L for Ca^{2+}.
3. The specimens prepared with 50 wt% seawater (SW) exhibited the highest piezoresistive sensitivity. This enhanced performance can be attributed to the optimal ion concentration within the pore solution, as observed in the 50 SW mixture, which facilitates more effective charge transport and improves the overall self-sensing capability of the material.

This work integrates the scientific understanding of hydration and conduction mechanisms with the practical objectives of developing seawater-based, self-sensing cementitious materials for sustainable infrastructure. The demonstrated piezoresistive performance highlights the potential of MWCNT–cement composites for traffic detection (TD) and structural health monitoring (SHM), particularly in coastal or marine environments where sustainability and durability are key priorities.

CRediT authorship contribution statement

Zhizhong Deng: Writing – original draft, Visualization, Validation, Methodology, Investigation, Formal analysis, Data curation, Conceptualization. **Daichao Sheng:** Writing – review & editing, Supervision, Project administration, Investigation, Funding acquisition. **Wengui Li:** Writing – review & editing, Investigation. **Quang Dieu Nguyen:** Writing – review & editing, Investigation, Formal analysis, Conceptualization, Resources, Supervision. **Aziz Hasan Mahmood:** Writing – review & editing, Investigation, Formal analysis.

Declaration of Competing Interest

The authors declare that they have no known competing financial interests or personal relationships that could have appeared to influence the work reported in this paper.

Acknowledgements

The authors appreciate the Australian Research Council (ARC), Australia (IH180100010) and University of Technology Sydney Research Academic Program at Tech Lab (UTS RAPT).

Data availability

Data will be made available on request.

References

[1] L. He, et al., "Research on the self-healing behavior of asphalt mixed with healing agents based on molecular dynamics method, Constr. Build. Mater. 295 (2021) 123430.
[2] H.B. Birgin, S. Laflamme, A. D'Alessandro, E. Garcia-Macias, F. Ubertini, "A weigh-in-motion characterization algorithm for smart pavements based on conductive cementitious materials, Sensors 20 (3) (2020) 659.
[3] B. Han, J. Ou, "Embedded piezoresistive cement-based stress/strain sensor, Sens. Actuators A Phys. 138 (2) (2007) 294–298.
[4] N. Asim, et al., "Application of graphene-based materials in developing sustainable infrastructure: An overview, Compos. B Eng. 245 (2022) 110188.
[5] S. Wen, D. Chung, "Cement-based controlled electrical resistivity materials, J. Electron. Mater. 30 (2001) 1448–1451.
[6] S. Rana, R. Fangueiro, A.G. Correia, "A review on smart self-sensing composite materials for civil engineering applications, AIMS Mater. Sci. 3 (2) (2016).
[7] C. Hong, Q. Li, Z. Zhuang, H. Xie, S. Xu, "Electrical and piezoresistive properties of ultra-high toughness cementitious composite incorporating multi-walled carbon nanotubes: Testing, analyzing, and phenomenological modeling, Cem. Concr. Compos. 154 (2024) 105757.
[8] A. Dinesh, S. Indhumathi, M. Pichumani, "Self-sensing cement composites for structural health monitoring: from know-how to do-how, Autom. Constr. 160 (2024) 105304.
[9] L. Shen, et al., "Factory-level measurements on CO2 emission factors of cement production in China, Renew. Sustain. Energy Rev. 34 (2014) 337–349.
[10] I. WBCSD, Cement Technology Roadmap 2009: carbon emissions reductions up to 2050, World Bus. Counc. Sustain. Dev. Int. Energy Agency (2009).
[11] K. Kupwade-Patil, M. Tyagi, C.M. Brown, O. Büyüköztürk, "Water dynamics in cement paste at early age prepared with pozzolanic volcanic ash and Ordinary Portland Cement using quasielastic neutron scattering, Cem. Concr. Res. 86 (2016) 55–62.
[12] B. Hannah, L. Martin, M. Uriarte, T. Haase, G. Ganapathi, F. Labarca, "Water usage optimization during concrete operations, World Environ. Water Resour. Congr. 2013 Showcasing Future (2013) 3114–3121.
[13] S.A. Miller, A. Horvath, P.J. Monteiro, "Impacts of booming concrete production on water resources worldwide, Nat. Sustain. 1 (1) (2018) 69–76.
[14] M.G. Chung, K.A. Frank, Y. Pokhrel, T. Dietz, J. Liu, "Natural infrastructure in sustaining global urban freshwater ecosystem services, Nat. Sustain. 4 (12) (2021) 1068–1075.
[15] D. Babor, D. Plian, L. Judele, "Environmental impact of concrete," *Buletinul Institutului Politehnic din Iasi*, Sect. Constr. Arhit. 55 (4) (2009) 27.
[16] W. Su, J. Liu, L. Liu, Z. Chen, C. Shi, "Progresses of high-performance coral aggregate concrete (HPCAC): A review, Cem. Concr. Compos. 140 (2023) 105059.
[17] P. Webb. Introduction to Oceanography, Roger Williams University, 2021.
[18] J. Harris. Non-Destructive Evaluation of Concrete Using Electrical Resistivity and Ultrasonic Wave Propagation, The University of Maine, 2022.
[19] Y. Bu, J. Weiss, "The influence of alkali content on the electrical resistivity and transport properties of cementitious materials, Cem. Concr. Compos. 51 (2014) 49–58.
[20] K.A. Snyder, X. Feng, B. Keen, T. Mason, "Estimating the electrical conductivity of cement paste pore solutions from OH−, K+ and Na+ concentrations, Cem. Concr. Res. 33 (6) (2003) 793–798.
[21] S. Masoumi, S. Zare, H. Valipour, M.J. Abdolhosseini Qomi, "Effective interactions between calcium-silicate-hydrate nanolayers, J. Phys. Chem. C. 123 (8) (2019) 4755–4766.
[22] A. Cheng, S.-J. Chao, W.-T. Lin, "Effects of leaching behavior of calcium ions on compression and durability of cement-based materials with mineral admixtures, Materials 6 (5) (2013) 1851–1872.
[23] C. Jiang, C. Song, X.-L. Gu, Q. Zhang, W.-P. Zhang, "Modeling electrochemical chloride extraction process in cement-based materials considering coupled multi-ion transports and thermodynamic equilibriums, J. Clean. Prod. 401 (2023) 136778.
[24] W. Su, et al., "Internal curing of fine coral aggregate in cement mortars with low water-to-cement ratio: difference in freshwater and seawater, Cem. Concr. Compos. 150 (2024) 105572.
[25] F.M. Nishat, I.B. Borno, A. Tahsin, W. Ashraf, "New insights into the interaction between seawater and CO2-activated calcium silicate composites, Cem. Concr. Compos. 157 (2025) 105929.
[26] Q. Fan, L. Fan, W.-M. Quach, J. Duan, "The impact of seawater ions on urea decomposition and calcium carbonate precipitation in the MICP process, Cem. Concr. Compos. 152 (2024) 105631.
[27] Z. Deng, A.H. Mahmood, W. Dong, D. Sheng, X. Lin, W. Li, "Piezoresistive performance of self-sensing bitumen emulsion-cement mortar with multi-walled carbon nanotubes, Cem. Concr. Compos. 153 (2024), https://doi.org/10.1016/j.cemconcomp.2024.105718.
[28] A. Standard, General purpose and blended cements, Standard Australian, *Sydney, Australia*, 2010.
[29] M.S. Konsta-Gdoutos, C.A. Aza, "Self sensing carbon nanotube (CNT) and nanofiber (CNF) cementitious composites for real time damage assessment in smart structures, Cem. Concr. Compos. 53 (2014) 162–169.
[30] A.S. f Testing, Materials. Standard Practice for the Preparation of Substitute Ocean Water, ASTM International, 2013.
[31] P. Li, et al., "Hydration of portland cement with seawater toward concrete sustainability: phase evolution and thermodynamic modelling, Cem. Concr. Compos. 138 (2023) 105007.
[32] R. Wang, F. He, C. Shi, D. Zhang, C. Chen, L. Dai, "AC impedance spectroscopy of cement - based materials: measurement and interpretation, Cem. Concr. Compos. 131 (2022), https://doi.org/10.1016/j.cemconcomp.2022.104591.
[33] H.-W.-X. Li, G. Lyngdoh, N.M.A. Krishnan, S. Das, "Machine learning guided design of microencapsulated phase change materials-incorporated concretes for enhanced freeze-thaw durability, Cem. Concr. Compos. 140 (2023), https://doi.org/10.1016/j.cemconcomp.2023.105090.
[34] F. Gulisano, T. Buasiri, F.R.A. Apaza, A. Cwirzen, J. Gallego, "Piezoresistive behavior of electric arc furnace slag and graphene nanoplatelets asphalt mixtures for self-sensing pavements, Autom. Constr. 142 (2022) 104534.
[35] A. C, "Standard test method for measurement of heat of hydration of hydraulic cementitious materials using isothermal conduction calorimetry. American Society of Testing and Materials, ASTM, West Conshohocken, PA, USA, 2015, pp. 1–9.
[36] Z. Shi, et al., "Friedel's salt profiles from thermogravimetric analysis and thermodynamic modelling of Portland cement-based mortars exposed to sodium chloride solution, Cem. Concr. Compos. 78 (2017) 73–83, https://doi.org/10.1016/j.cemconcomp.2017.01.002.
[37] K.L. Scrivener, A. Nonat, "Hydration of cementitious materials, present and future, Cem. Concr. Res. 41 (7) (2011) 651–665.

[38] Y. Zhao, X. Hu, C. Shi, Q. Yuan, D. Zhu, "Determination of free chloride in seawater cement paste with low water-binder ratio, Cem. Concr. Compos. 124 (2021), https://doi.org/10.1016/j.cemconcomp.2021.104217.
[39] F. Qu, W. Li, K. Wang, V.W. Tam, S. Zhang, "Effects of seawater and undesalted sea sand on the hydration products, mechanical properties and microstructures of cement mortar, Constr. Build. Mater. 310 (2021) 125229.
[40] Y. Sun, et al., "Mechanisms on accelerating hydration of alite mixed with inorganic salts in seawater and characteristics of hydration products, ACS Sustain. Chem. Eng. 9 (31) (2021) 10479–10490.
[41] S.A. Yaseen, G.A. Yiseen, C.S. Poon, Z. Li, "Influence of seawater on the morphological evolution and the microchemistry of hydration products of tricalcium silicates (C3S), ACS Sustain. Chem. Eng. 8 (42) (2020) 15875–15887.
[42] A.M. Ragab, M.A. Elgammal, O.A. Hodhod, T.E. Ahmed, "Evaluation of field concrete deterioration under real conditions of seawater attack, Constr. Build. Mater. 119 (2016) 130–144.
[43] B. Lu, C. Shi, J. Zhang, J. Wang, "Effects of carbonated hardened cement paste powder on hydration and microstructure of Portland cement, Constr. Build. Mater. 186 (2018) 699–708.
[44] G. Tartaglione, D. Tabuani, G. Camino, "Thermal and morphological characterisation of organically modified sepiolite, Microporous Mesoporous Mater. 107 (1-2) (2008) 161–168.
[45] F. Jin, A. Al-Tabbaa, "Thermogravimetric study on the hydration of reactive magnesia and silica mixture at room temperature, Thermochim. Acta 566 (2013) 162–168.
[46] P. Li, W. Li, T. Yu, F. Qu, V.W.Y. Tam, "Investigation on early-age hydration, mechanical properties and microstructure of seawater sea sand cement mortar, Constr. Build. Mater. 249 (2020), https://doi.org/10.1016/j.conbuildmat.2020.118776.
[47] A.F. Sosa Gallardo, J.L. Provis, "Electrochemical cell design and impedance spectroscopy of cement hydration, J. Mater. Sci. 56 (2) (2021) 1203–1220.
[48] J. Wen, Electrochem. impedance Spectrosc. Cem. Based Mater." UC Irvine (2020).
[49] Z. Deng, Q.D. Nguyen, A.H. Mahmood, Y. Pang, T. Shi, D. Sheng, "Piezoresistivity assessment of self-sensing asphalt-based pavements with machine learning algorithm, Constr. Build. Mater. 468 (2025) 140291.
[50] P. Li, W. Li, Z. Sun, L. Shen, D. Sheng, "Development of sustainable concrete incorporating seawater: A critical review on cement hydration, microstructure and mechanical strength, Cem. Concr. Compos. 121 (2021), https://doi.org/10.1016/j.cemconcomp.2021.104100.
[51] P. Zhan, J. Xu, J. Wang, J. Zuo, Z. He, "Structural supercapacitor electrolytes based on cementitious composites containing recycled steel slag and waste glass powders, Cem. Concr. Compos. 137 (2023), https://doi.org/10.1016/j.cemconcomp.2022.104924.
[52] D. Wang, et al., "Nano-structure and sensitivity of self-sensing geopolymer composites containing nano carbon black, Cem. Concr. Compos. (2025) 106072.
[53] Y. Cheng, H. Yu, B.-l Zhu, D.-x Wei, "Laboratory investigation of the strength development of alkali-activated slag-stabilized chloride saline soil, J. Zhejiang Univ. Sci. A 17 (5) (2016) 389–398.
[54] Y. Cai, Y. Tao, D. Xuan, Y. Sun, C.S. Poon, "Effect of seawater on the morphology, structure, and properties of synthetic ettringite, Cem. Concr. Res. 163 (2023) 107034.
[55] F. Chen, S. Tong, H. Wang, W. Chen, "Influence of seawater erosion on the strength and pore structure of cement soil with ferronickel slag powder, Coatings 13 (1) (2023) 100.
[56] W. Dong, W. Li, Z. Tao, K. Wang, "Piezoresistive properties of cement-based sensors: Review and perspective, Constr. Build. Mater. 203 (2019) 146–163, https://doi.org/10.1016/j.conbuildmat.2019.01.081.
[57] M.S. Konsta-Gdoutos, Z.S. Metaxa, S.P. Shah, "Highly dispersed carbon nanotube reinforced cement based materials, Cem. Concr. Res. 40 (7) (2010) 1052–1059, https://doi.org/10.1016/j.cemconres.2010.02.015.
[58] S. Musso, J.-M. Tulliani, G. Ferro, A. Tagliaferro, "Influence of carbon nanotubes structure on the mechanical behavior of cement composites, Compos. Sci. Technol. 69 (11-12) (2009) 1985–1990.
[59] B. Han, X. Yu, E. Kwon, "A self-sensing carbon nanotube/cement composite for traffic monitoring, Nanotechnology 20 (44) (2009) 445501.
[60] A.M. Mohamed, B.A. Tayeh, S.S. Majeed, Y.I.A. Aisheh, M.N.A. Salih, "Fresh, hardened, durability and microstructure properties of seawater concrete: A systematic review, J. CO2 Util. 83 (2024) 102815.
[61] A. D'Alessandro, F. Ubertini, A.L. Materazzi, S. Laflamme, M. Porfiri, "Electromechanical modelling of a new class of nanocomposite cement-based sensors for structural health monitoring, Struct. Health Monit. 14 (2) (2015) 137–147.
[62] S. Qin, D. Zou, T. Liu, A. Jivkov, "A chemo-transport-damage model for concrete under external sulfate attack, Cem. Concr. Res. 132 (2020) 106048.
[63] Y. Zhang, S. Cao, J. Chang, S. Ding, Q. Zhao, C.S. Poon, "Influence of seawater on the microstructure of calcium-silicate-hydrate (CSH) gels with varying Ca/Si ratios based on alite-silicon dioxide system, Cem. Concr. Compos. (2025) 106251.
[64] Y. Cao, L. Guo, B. Chen, J. Wu, "Thermodynamic modelling and experimental investigation on chloride binding in cement exposed to chloride and chloride-sulfate solution, Constr. Build. Mater. 246 (2020) 118398.